TRANSVERSE EMITTANCE RECONSTRUCTION ALONG THE CYCLE OF THE CERN ANTIPROTON DECELERATOR

G. Russo*, B. Dupuy, D. Gamba, L. Ponce
CERN, Geneva, Switzerland

Abstract

The precise knowledge of the transverse beam emittances on the different energy plateaus of the CERN Antiproton Decelerator (AD) ring is important for assessing and optimising the machine performance as well as its setting-up. This paper presents a methodology for reconstructing transverse beam profiles from scraper measurements employing the Abel Transform (AT). The proposed methodology provides a precise, reproducible and user independent way of computing the beam emittance, as well as a useful tool to qualitatively track machine performance in routine operation. As discussed in this paper, its application has already been proven crucial for the operational setting-up of the stochastic cooling in AD. It also opens up the possibility for detailed benchmark studies of the cooling performance in different machine and beam conditions.

INTRODUCTION

The Antiproton Decelerator (AD) ring is the only operational facility worldwide where high brightness antiproton beams are produced. Nowadays the AD ring reaches a nominal intensity of $4.0 \times 10^7 \bar{p}$ in a single bunch, which is decelerated from the production momentum of $3.574 \, \text{GeV/c}$ to $100 \, \text{MeV/c}$. Over the years, AD has undergone many significant changes and upgrades, however one of the main remaining challenges is the determination of the transverse emittance along the cycle. Conversely to accelerators, the geometric emittance adiabatically increases during the deceleration process by a factor proportional to the ratio between initial and final beam momentum; therefore, stochastic and electron cooling is applied on several energy plateaus. From here the need to be able to characterise the emittance along the AD cycle as a mean to control the performance of the cooling systems arises.

EMITTANCE MEASUREMENTS

Emittance along the AD cycle can be measured by means of a scraper and Ionization Profile Monitors (IPM). In this paper, only the former will be analysed since the latter is presently not operational. It is worth mentioning that, given the length of the AD cycle ($\approx 110 \text{s}$) and given that a scraper measurement leads to a complete loss of the beam, the time needed to perform a complete set of emittance measurements in the horizontal (H) and vertical (V) plane at a few key moments along the cycle can take between 45 minutes and up to 2 hours, if no machine downtime occurs in the meantime.
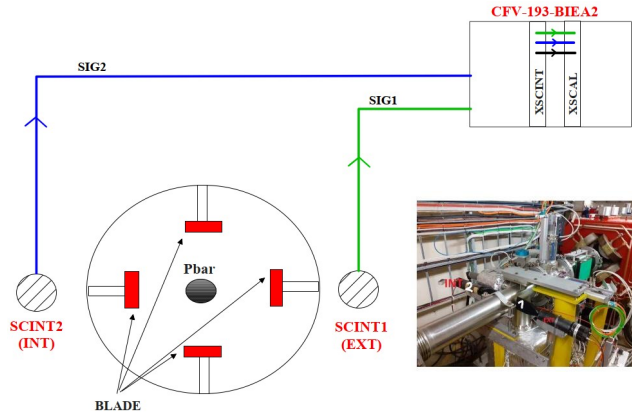
* giulia.russo@cern.ch

Figure 1: Schematic representation of the 4 blades systems used for scraper measurements as well as a photo of the system in the AD ring.

In AD four independent scraper blades (see Fig. 1), two per plane, are installed and each of them has its own moving mechanism. As the blade moves inside the beam, portions of the beam are scraped away. The interaction of $\bar{p}$ and the blade produces secondary particles that are detected by two scintillators (namely, SCINT1 and SCINT2) installed symmetrically outside the vacuum chamber in a horizontal arrangement, as shown in Fig. 1. The signal of one of the two scintillators is further processed by means of an electronic scalar board which provides a signal with a higher sampling rate

For a $4D$ Gaussian beam it is possible to analytically compute the profile of the losses during the scraping process. If the scraper is installed in a dispersion-free region (as in AD), the evolution of the losses as a function of the scraper position reads as:

$$\ell(u_s) = \frac{u_s - u_0}{\beta_u(s = s_s)\epsilon_{u, \text{RMS}}} \exp\left(-\frac{1}{2}\frac{(u_s - u_0)^2}{\beta_u(s = s_s)\epsilon_{u, \text{RMS}}}\right),$$
(1)

where u refers to x or y whether the Horizontal (H) or Vertical (V) plane is considered, respectively, and u_s indicates the scraper position and u_0 the beam closed orbit. This process can also be simulated numerically. If a fictitious scraper is moved along the H plane (and the same holds true for the V one) then it progressively removes particles with action J larger than J_{max}:

$$2\epsilon_{\text{RMS}} = <2J_{\text{max}}> = <X^2 + X'^2> = <\frac{(x_s - x_0)^2}{\beta_x}>, \quad (2)$$
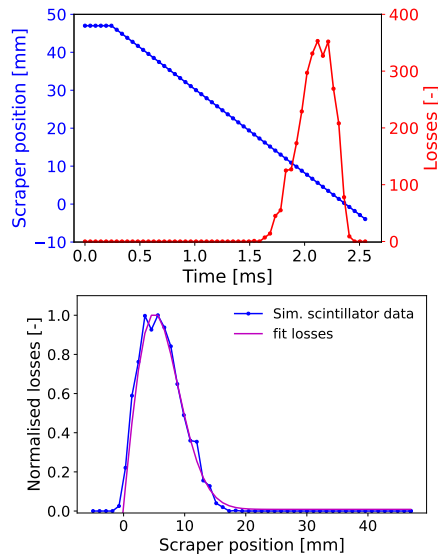
Figure 2: Top: evolution of the scraper position (blue) and losses (red) as a function of time. Bottom: from the knowledge of the scraper velocity it is possible to determine the loss evolution as a function of the scraper position. The simulated data is then fit to Eq. (1).

where X and X' are the particles coordinate in normalised phase-space, defined as [1]:

$$\begin{cases} X = \frac{1}{\sqrt{\beta_x}}x, \\ X' = \frac{\alpha_x}{\sqrt{\beta_x}}x + \sqrt{\beta_x}x'. \end{cases}$$

As the scraper speed is much slower than the particle motion in phase space due to betatron oscillations, particles are scraped according to their action J_x. Figure 2 shows an example of the simulated evolution of the scraper position and losses as a function of the time or scraper position. It is straightforward to determine what is the loss profile as a function of the scraper position (as shown in Fig. 2 bottom) in this ideal numerical simulation. Equation (1) can be used to fit the loss profile and reconstruct the original H emittance of the 4D Gaussian beam. In this example, the difference between the fitted emittance and the original one is about 3%.

Systematic effects and system imperfections make this reconstruction more challenging with real data coming from the AD scraper system. In AD, once the beam is completely scraped off, the two detectors provide a signal that is directly proportional to the number of particles lost, which can be directly related to the beam emittance according to Eq. (1). However, synchronization between scraper movement and loss detection is not possible at the moment. Therefore, from a single scraper measurement is not possible to determine the beam closed orbit position. The directly translation of losses as a function of time into losses as a function of scraper position is, at the moment, not feasible. Instead, it is possible to multiply the time recorded by the scintillator by the scraper velocity. This allows to have the evolution of the losses as a function of an "equivalent" scraper position. This issue is planned to be solved in the future to be able to
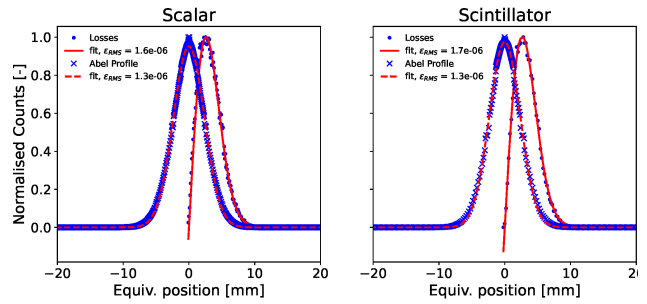

Figure 3: The loss profile from the scalar (left) and the scintillator (right) are shown as a blue dot. The data are fit to Eq. (1) to obtain the RMS emittance and the result of the fit is shown with a continuous red line. The AT on the losses provides a profile (blue crosses) which is fitted to a Gaussian curve (red dashed line) from which value of RMS emittance is retrieve.

measure the beam orbit position and the emittance with a single scraper measurement.

An alternative way of looking at the loss profile is to transform it into the transverse beam profile using the Abel Transform (AT) [2]. From this the transverse beam emittance can be determined, for example by performing a simple Gaussian fit. An AT has been implemented, tested and benchmarked in Python and then translated in JAVA to integrate it in the standard operational tools used in the control room. The new implementation has additional features compared to the PyAbel library of Python [3], namely, the possibility to over-sample data over a range defined by the user, helpful for AD low-energy emittance measurements, as well as to automatically detect the start of the loss profile.

An example of a real scraper measurements at the beginning of the 2.001 GeV/c plateau is shown in Fig. 3, where the signal from the scalar board (left), a digitiser introduced a few years ago to provide better resolution signals, and one of the two scintillators (right) are reported. The values of the RMS emittance are retrieved from the fit of the losses using Eq.(1) and from a Gaussian fit on the Abel profile. The values obtained are compatible between the two instruments, as well as between the Gaussian fit on the Abel profiles and the loss fit. These results allow us to use this procedure to assess the emittance along the AD cycle.

AD EMITTANCE EVOLUTION

The AT procedure as been adopted as a standard tool from March 2023, and since then several measurements have been taken to assess the emittance evolution over the AD cycle. The fit procedure based on the use of Eq. (1) is not available in the standard operation tool used in the control room, but it is used in post processing to validate the values obtained from the Gaussian fit of the AT profile, as shown in Fig. 3.

Figure 4 shows the emittance measurements in the V (top) and H (bottom) plane along the AD cycle carried out in 2022 and in 2023. In this figure the type of cooling (stochastic cooling, SC, or electron cooling, EC) and its time-window are indicated by the light purple areas. The emittance is

Table 1: SC performance: evaluation of the emittance ratio between the start and the end of the energy plateau, compared to design values.

p [GeV/c]	Ref. [8]	H [-]		V [-]	
		2022	2023	2022	2023
3.574	40 (H, V)	N. A.	43	N. A.	23
2.001	1.8 (H, V)	0.89	1.5	1.8	1.3

has a significant worsening of performance in the H plane while the V plane performance is almost unchanged. It is worth mentioning that a change of optics is performed at the end of the 2.001 GeV/c plateau, which could be a source of emittance blowup. The hardware changes between 2022 and 2023 discussed above might explain this worsening, and work is ongoing to recover the previous performance. Finally, the last deceleration ramp has been improved in the V plane with a worsening in the H plane. Also in this case, studies are ongoing.

Stochastic Cooling

The SC occurs on the two highest energy flat portions of the AD cycle and aims at reducing both longitudinal and transverse beam emittances [5]. The AD SC system has been significantly improved over the years, and additional studies are ongoing to further improve its performance. Additional information on these topics can be found in Refs. [5–7]. The cooling process is not adiabatic and it allows to reduce emittances without loosing particles. The emittance reduction factors along the two stochastic cooling plateaus obtained from recent emittance measurements provide information on cooling performance: the higher the reduction factor, the more the emittance is reduced over the plateau. The results from the present measurements are summarised in Table 1, together with expected values from the AD design reports [6, 8]. In 2022 no emittance measurements were take right after injection, therefore, it is not possible to assess the SC performance in 2022 for the injection energy. However, it is possible to notice that in 2023 both the H and V normalised emittance at the end of the 3.574 GeV/c plateau have been significantly reduced compared to 2022 (by a factor 1.7 and 4.7 in the V and H plane, respectively). Along the 2.001 GeV/c plateau the performance has been significantly improved in the H plane, while a slight worsening occurs in the V plane.

Electron Cooling

Electron cooling is performed at the two lowest energy plateaus of the AD cycle after the optics change, namely at 300 MeV/c and at 100 MeV/c [8, 9]. Similarly to the
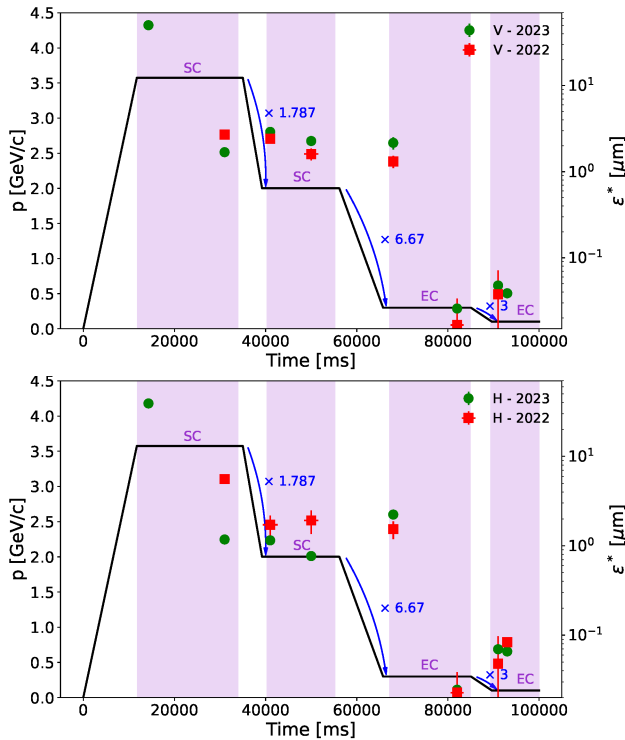

Figure 4: Normalised V (top) and H (bottom) emittance measurements over the AD cycle performed during the 2022 run (red) and the 2023 run (green).

shown in its normalised form, therefore removing the energy dependence. In this way non-adiabatic processes are clearly visible. Note that the 2022 data has been re-analysed using the AT procedure. The difference in emittance between 2022 and 2023 might be due to hardware changes introduced in between the two runs, in particular:

- during the 2022 run a power supply that provides dipolar compensation of some of the ring dipoles has failed and the entire physics program has been carried out providing this compensation using standard orbit correctors.

- a special ring quadrupole [4], QFC54, failed at the start of the 2023 run and had to be refurbished with new coils.

The actual reasons are still to be investigated, and this shows the importance of having reliable emittance measurements. The main observations drawn from the data presented in Fig. 4 are detailed in the following subsections.

Deceleration Segments

During deceleration the physical emittance of the beam increases adiabatically [1], while the normalised emittance, as in Fig. 4, is expected to remain constant. An increase in the normalised emittance, as it is observed in Fig. 4, highlights thus an unwanted blow-up during deceleration. The overall performance has been significantly improved between 2022 and 2023 along the first deceleration ramp, with only a slight worsening in the V plane. The second deceleration ramp

Table 2: EC performance: evaluation of the emittance ratio between the start and the end of the energy plateau.

p [MeV/c]	Ref. [8]	H [-]		V [-]	
		2022	2023	2022	2023
300	16.5 (H, V)	67	91	79	84
100	6 (H, V)	0.57	1.1	N. A.	1.2

SC, the assessment of the EC performance can be done evaluating the reduction of emittance between the start and the end of the plateaus. The results are reported in Table 2. The 300 MeV/c plateau has better performance than those predicted in Ref. [8], while the 100 MeV/c one seems to be worse. However, this last plateau is more complicated to study since the $\bar{p}$ orbit shifts by approximately 10 mm along the plateau. A set of scraper measurements at different timings has been taken to evaluate the evolution of the beam core and beam tails during the cooling process. Figure 5 shows the normalised and cumulative beam losses for several scraper measurements at different times along the plateau in both transverse planes. The color code represents the time at which the beam scraping is started. The higher the timing the longer the beam is cooled before scraping. In the V plane no significant changes of the core width are observed, while, as the time increases, more and more particles with intermediate action are cooled towards the core. However, in the H plane, reductions and increases in the beam core width are observed, together with a non-optimal tails cooling after ≈ 93000 ms, as shown in Fig. 5 bottom left. In this case defining the emittance is difficult. From the cumulative losses the emittance can be defined as area that encloses 95% of particles, divided by 6 [1]. However, this definition would bring to have an emittance of $\approx 2.5\mu m$ in H and $\approx 3\ \mu m$ in V, which is significantly different from those obtained if only the core is considered, namely 0.9 µm in H and $\approx 0.4\ \mu m$ in V. These studies highlight the need to perform systematic analysis to possibly optimize the tails cooling.
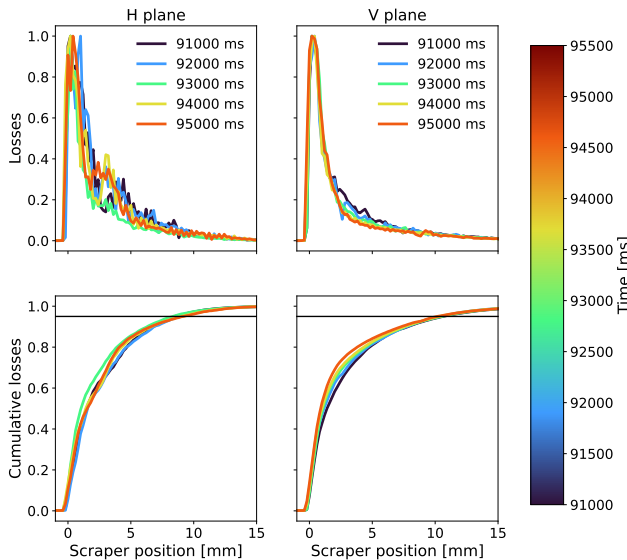

Figure 5: Tails evolution along the 100 MeV/c plateau. Top: normalised scraper losses as a function of time. Bottom: cumulative losses, where the 95% of the beam lost is reported with a black line.

ACCEPTANCE MEASUREMENTS

Transverse acceptance measurements provide important information on the maximum single-particle emittance that can be transmitted [1, 10, 11]. Recent measurements have been carried out to verify the present value of AD acceptance both at injection and extraction energies. The procedure adopted to measure acceptance is the same for the two energies. Once the beam reaches the desired energy plateau it is initially cooled by the SC or EC, then cooling is stopped and the beam is excited by means of the tune meter. Once beam losses are observed, meaning that the beam has occupied the entire acceptance, a scraper measurement is performed. To assess the acceptance, namely the maximum action according to Eq. (2), and inserting for $x_s - x_0$ the width of the region of scraper position, over which losses occur. The results of these measurements are reported in Table 3 where acceptance is in mm mrad unit. The H acceptance at 100 MeV/c is significantly smaller than the V one. This was the first time that acceptance measurements were taken at the AD extraction energy, and the smaller horizontal acceptance could be linked to reduced aperture near the electron cooler at low energy.

Table 3: Acceptance and its error for the AD injection and extraction energies.

p [GeV/c]	H [µm]		V [µm]	
	2002	2023	2002	2023
3.574	180 [12]	160±16	200 [12]	125±17
0.100	N. A.	68±5	N. A.	153±21

SPACE CHARGE TUNE SHIFT

A first estimation of the maximum space charge tune shift [13] as a function of energy in AD was obtained. As the energy of $\bar{p}$ is reduced, the tune shift increases. At injection energy the maximum space charge tune shift is -1.8×10^{-7} and -8.9×10^{-7} for the H and V planes, respectively. It starts to become more relevant at 300 MeV/c where the maximum values reaches -0.002 and -0.003 for the H and V plane, respectively; and it becomes even larger at the extraction energy, -0.01 for the H plane and -0.02 for the V plane. The associated emittance growth rates and intra beam scattering effects are still to be evaluated, and will be subject of future studies.

CONCLUSIONS

A new robust method for measuring the transverse beam emittance, based on the use of the AD scraper system, has been developed. Its systematic application along the cycle has been proven fundamental to assess the performance of the stochastic and electron cooling techniques, as well as the preservation of the normalized emittances during deceleration. Performing these measurements periodically as well as re-analysing previous years data allows to determine AD performance over the years. In conclusion, studies are needed to improve the deceleration and the EC performance along the last energy plateau, where larger discrepancies from previous years performance and design report data have been observed.

THC1C1

REFERENCES

[1] S. Y. Lee, *Accelerator Physics*, Singapore, World Scientific Publishing Co. Ltd., 2004. `doi:10.1142/11111`

[2] C. Carli, A. Jansson, M. Lindroos, H. Schonauer, "A comparative study of profile and scraping methods for emittance measurements in the PS Booster", CERN, Geneva, Switzerland, Rep. CERN, PS-2000-062-OP, 2000.

[3] S. Gibson, D. D. Hickstein, R. Yurchak, M. Ryazanov, DD. Das, G. Shih, PyAbel/PyAbel: v0.9.0 (v0.9.0), Zenodo, 2022. `doi:10.5281/zenodo.7438595`

[4] M. Battiaz, M. Harold, G. Suberlucq, H.-H. Umstatter, "A strong focusing benging magnet for the CERN Antiproton Collector", CERN, Geneva, Switzerland, Rep. CERN-PS-87-22-AA, 1987, `http://cds.cern.ch/record/175881/`.

[5] S. Van der Meer, "Stochastic cooling theory and devices", 1978, `https://cds.cern.ch/record/133586/`.

[6] S. Baird *et al.*, "Design study of the antiproton decelerator: AD", CERN, Geneva, Switzerland, Rep. CERN-PS-96-43-AR, 1996, `https://cds.cern.ch/record/2831065/`.

[7] W. Höfle, C. Carli, F. Caspers, B. Dupuy, F. Gamba, R. Louwerse, V.R. Myklebust, J.C Oliveira, L. Ponce, S. Rey, L. Thorndahl, "Recommissioning of the CERN AD Stochastic Cooling System in 2021 after Long Shutdown 2", in *Proc. COOL'21*, Novosibirsk, Russia, Nov. 2021, pp. 20–25. `doi:10.18429/JACoW-COOL2021-S302`

[8] S. Maury, "The antiproton decelerator (AD)", CERN, Geneva, Switzerland, Rep. CERN-PS-99-50-HP, 1999, `http://cds.cern.ch/record/2850009/`.

[9] D. Gamba and L. Bojtár and C. Carli and B. Dupuy and A. Frassier and L.V. Jørgensen and L. Ponce and G. Tranquille, "AD/ELENA Electron Cooling Experience During and after CERNs Long Shutdown (LS2)", in *Proc. COOL'21*, Novosibirsk, Russia, Nov. 2021, pp. 36–41. `doi:10.18429/JACoW-COOL2021-S503`

[10] E. J. N. Wilson, "Transverse beam dynamics", *CAS - CERN Accelerator School: Intermediate Accelerator Physics*, pp. 1-30, 2006. `doi:10.5170/CERN-2006-002.1`

[11] D. Mohl, "Sources of emittance growth", *CAS - CERN Accelerator School: Intermediate Accelerator Physics*, pp. 245-270, 2006. `doi:10.5170/CERN-2006-012.45`

[12] P. Belochitskii, T. Eriksson, A. Findlay, E-B Holzer, R. Maccaferri, S. Maury, S. Pasinelli, F. Pedersen, G. Tranquille, "Two years of AD operation: Experience and progress", CERN, Geneva, Switzerland, Rep. CERN/PS 2002-046 (OP), 2002, `https://cds.cern.ch/record/567353/`.

[13] K. Schindl, "Space Charge", *CAS - Accelerator School: Intermediate Course on Accelerator Physics*, pp.305-320, 2006. `doi:10.5170/CERN-2006-002.305`